

Ice shelf advance and retreat rates along the coast of Queen Maud Land, Antarctica

K. T. Kim,¹ K. C. Jezek,² and H. G. Sohn³

Byrd Polar Research Center, The Ohio State University, Columbus, Ohio

Abstract. We mapped ice shelf margins along the Queen Maud Land coast, Antarctica, in a study of ice shelf margin variability over time. Our objective was to determine the behavior of ice shelves at similar latitudes but different longitudes relative to ice shelves that are dramatically retreating along the Antarctic Peninsula, possibly in response to changing global climate. We measured coastline positions from 1963 satellite reconnaissance photography and 1997 RADARSAT synthetic aperture radar image data for comparison with coastlines inferred by other researchers who used Landsat data from the mid-1970s. We show that these ice shelves lost $\sim 6.8\%$ of their total area between 1963 and 1997. Most of the areal reduction occurred between 1963 and the mid-1970s. Since then, ice margin positions have stabilized or even readvanced. We conclude that these ice shelves are in a near-equilibrium state with the coastal environment.

1. Introduction

Ice shelves are vast slabs of glacier ice floating on the coastal ocean surrounding Antarctica. They are a continuation of the ice sheet and form, in part, as glacier ice flowing from the interior ice sheet spreads across the ocean surface and away from the coast. The boundary between ice shelf and interior ice sheet is termed the grounding line and identifies the location where the glacier ice just goes afloat. The seaward ice shelf margin position is determined by the balance between iceberg-calving rates and the forward advection of upstream ice.

By their nature, ice shelves represent a boundary between ocean, atmosphere, and interior ice sheet. This configuration is believed to make ice shelves sensitive indicators of changing coastal environment. In 1978, Mercer predicted that one sign of a CO₂-induced climate-warming trend would be the retreat of ice shelves on the Antarctic Peninsula [Mercer, 1978]. Evidence in support of his prediction comes from the sustained retreat of the Wordie Ice Shelf from the late 1970s through the 1980s [Doake and Vaughan, 1991]. In early 1995 the northern Larsen Ice Shelf disappeared within a few days following a single storm [Rott et al., 1996].

In this paper, we investigate the extent of ice shelves fringing Queen Maud Land, ranging from the Fimbul Ice Shelf in the west to the Shirase Glacier in the east. These ice shelves are of interest because they are similar in size to the Antarctic Peninsula ice shelves, they are similarly constrained by numerous ice rises and coastal embayments, and they lie near the southerly limit of retreating Antarctic Peninsula ice shelves. Unlike the Antarctic Peninsula, these ice shelves exist in a generally colder climate and lie $\sim 7^\circ$ of latitude to the south of the

summer 0° isotherm [Tolstikov, 1966, p. 76; King and Turner, 1997, p. 141]. Following Mercer's hypothesis, we might expect these ice shelves to be relatively stable at the present time.

Following the approach of other investigators [Rott et al., 1996; Ferrigno et al., 1998; Skvarca et al., 1999], we compare the position of ice shelf margins and grounding lines derived from several high-resolution data sets acquired over the past 34 years. We use orthorectified (orthogonal-projected, relief-corrected, and uniform-scaled) 1963 Declassified Intelligence Satellite Photography (DISP) [McDonald, 1995], the 1973–1976 Antarctic Digital Database (ADD) [Cooper et al., 1993], and the 1997 RADARSAT-1 synthetic aperture radar (SAR) image mosaic [Jezek, 1998] to assess changes in ice shelf margin position and ice shelf area.

2. Queen Maud Land Ice Shelves

We are concerned with the ice shelves flanking the Atlantic coast sector of Antarctica as described by Swithinbank [1988]. Ice feeding the Queen Maud Land ice shelves flows downward from the East Antarctica plateau through an extensive range of east-west trending mountains across New Schwabenland (Figure 1). In the west, ice flows outward onto a long textured plain characterized by blue ice ablation regions near the grounding line [Liston et al., 2000]. Here we assume the abrupt change from crenellated to smooth surface to be the location of the ice shelf grounding line (Figure 2). Seaward of the grounding line, the smooth surfaces of the ice shelves are interrupted only by crevasses and rounded ice rises described in detail by Orheim [1978] and further described by Zwally et al. [1987]. Between $\sim 5^\circ\text{W}$ and $\sim 15^\circ\text{E}$ longitude the ice flows between the ice rises and forms extended ice tongues, the longest being an extension of the Jutulstraumen Glacier. From 15°E longitude to the Shirase Glacier the ice shelves are more confined to embayments formed between coastal and near-coastal promontories such as the Riiser-Larsen Peninsula. Along this entire stretch of coastline the ice sheet ends primarily at the terminus of ice shelves. Occasionally, the northerly extent is determined by the position of an ice rise or an ice-covered promontory such as the Riiser-Larsen Peninsula. The coastal ocean is covered by seasonal sea ice and temporally varying extents of fast ice.

¹Also at Department of Civil and Environmental Engineering and Geodetic Science, The Ohio State University, Columbus, Ohio.

²Also at Department of Geological Sciences, The Ohio State University, Columbus, Ohio.

³Also at Department of Civil Engineering, Yonsei University, Seoul, Korea.

Copyright 2001 by the American Geophysical Union.

Paper number 2000JC000317.
0148-0227/01/2000JC000317\$09.00

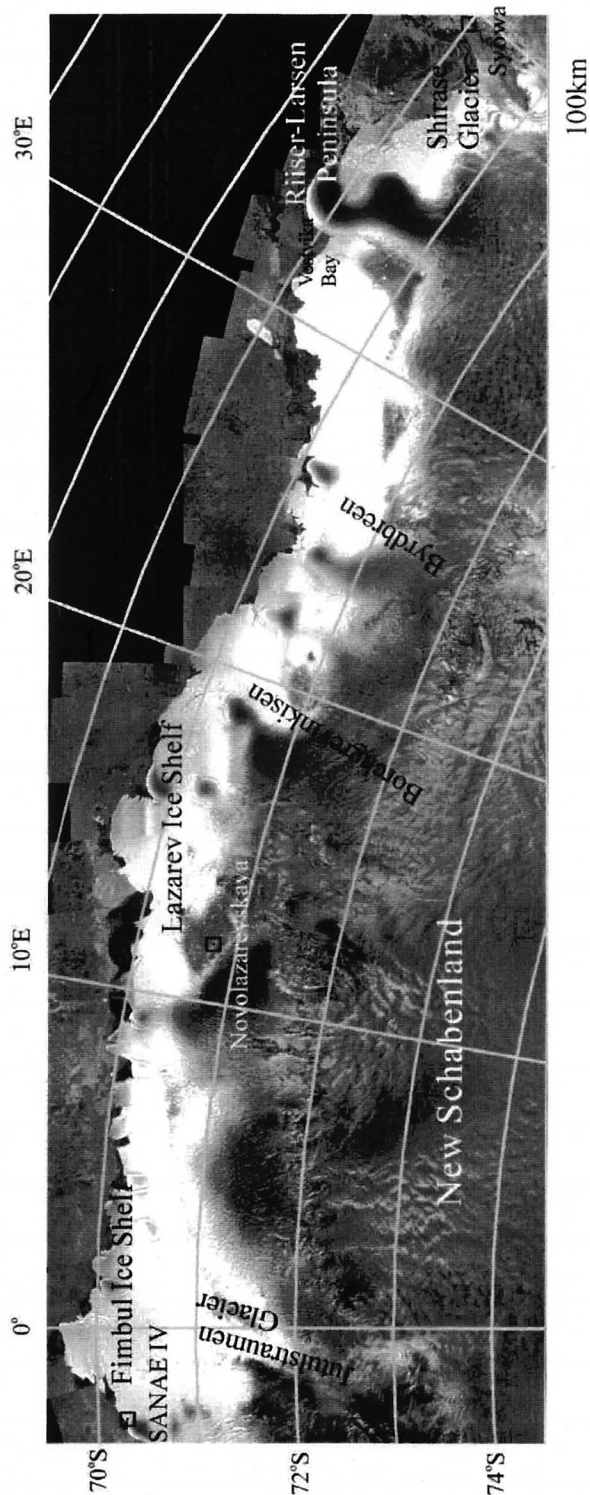


Figure 1. RADARSAT-1 SAR mosaic of the study area. Place names are referenced in the text.

Cold, katabatic winds from the East Antarctica plateau couple the temperature regime of the inland ice sheet with the coastal ice shelves. Over the period 1959–1996, mean annual temperatures at SANAE IV (70.3°S, 2.4°W, established by South African National Antarctic Expeditions), Novolazarevskaya (70.8°S, 11.8°E), and Syowa (69°S, 39.6°E) stations were -16.9° , -10.3° , and -10.5° C, respectively. Analyses of mean annual temperatures from these three stations show a consistent warming trend of between $\sim 0.012^{\circ}$ C per year for SANAE IV and Syowa and $\sim 0.03^{\circ}$ C per year for Novolazarevskaya [Jacka and Budd, 1998]. This is similar to areally averaged warming trends for the eastern part of the study area reported by Weller [1998]. For the westernmost part of the study area, Weller reports cooling trends of -0.02° C per year. In comparison, Jacka and Budd [1998] report a mean annual surface temperature of 0° C and a 0.024° C per year warming trend for the Antarctic Peninsula. For the period 1944–1991, Jacobs and Comiso [1993] report an annual average temperature for the western Antarctic Peninsula of $\sim -5^{\circ}$ C with a warming trend of 0.05° C per year.

3. Data Description

3.1. RADARSAT-1 SAR Data

RADARSAT-1 SAR data were acquired over Antarctica between September 19 and October 14, 1997. The coverage is complete and has been used to construct a seamless 25-m resolution image mosaic of Antarctica [Jezek, 1999]. For this analysis we used a 100-m (pixel size) orthorectified mosaic displayed as a polar stereographic projection with a standard parallel of 71° S. The SAR data were orthorectified using the Ohio State University (OSU) digital elevation model (DEM) of Antarctica described by Liu *et al.* [1999]. The DEM has an accuracy of ~ 35 m for the steeper portions of the ice sheet. Image rectification was further constrained by a network of ground control points obtained in cooperation with the Environmental Research Institute of Michigan and the National Imagery and Mapping Agency. The horizontal geolocation accuracy of the SAR mosaic over ice-covered terrain is estimated to be ~ 100 m [Noltimier *et al.*, 1999]. Consequently, we assign a 35-m vertical accuracy and a 100-m horizontal accuracy to points identified on the SAR mosaic. As discussed in section 3.4, these points are used to rectify the DISP images.

The part of the RADARSAT-1 SAR mosaic used in this study is shown in Figure 3a. The higher elevation interior ice sheet (lower region of Figure 3a) and some of the coastal promontories appear dark, indicating that the surface consists of dry snow [Fahnestock *et al.*, 1993; Jezek, 1999]. Most of the ice shelves and ice rises appear bright, which is a characteristic of refrozen seasonal melt areas. The seasonal sea ice cover is darker than the ice shelf, making the ice margin relatively easy to identify.

3.2. Antarctic Digital Database

The Scientific Committee on Antarctic Research ADD is a comprehensive digital collection of vector cartographic data of Antarctica. The ADD coastline used in this study is described by British Antarctic Survey *et al.* [1993] and by Thomson and Cooper [1993]. They note that reference data used to compile the ADD Queen Maud Land coastline comes from a variety of sources. These include coastlines supplied by the Institut für Angewandte Geodäsie (IFAG) for the sector west of 0° longitude and coastlines derived by Charles Swithinbank from

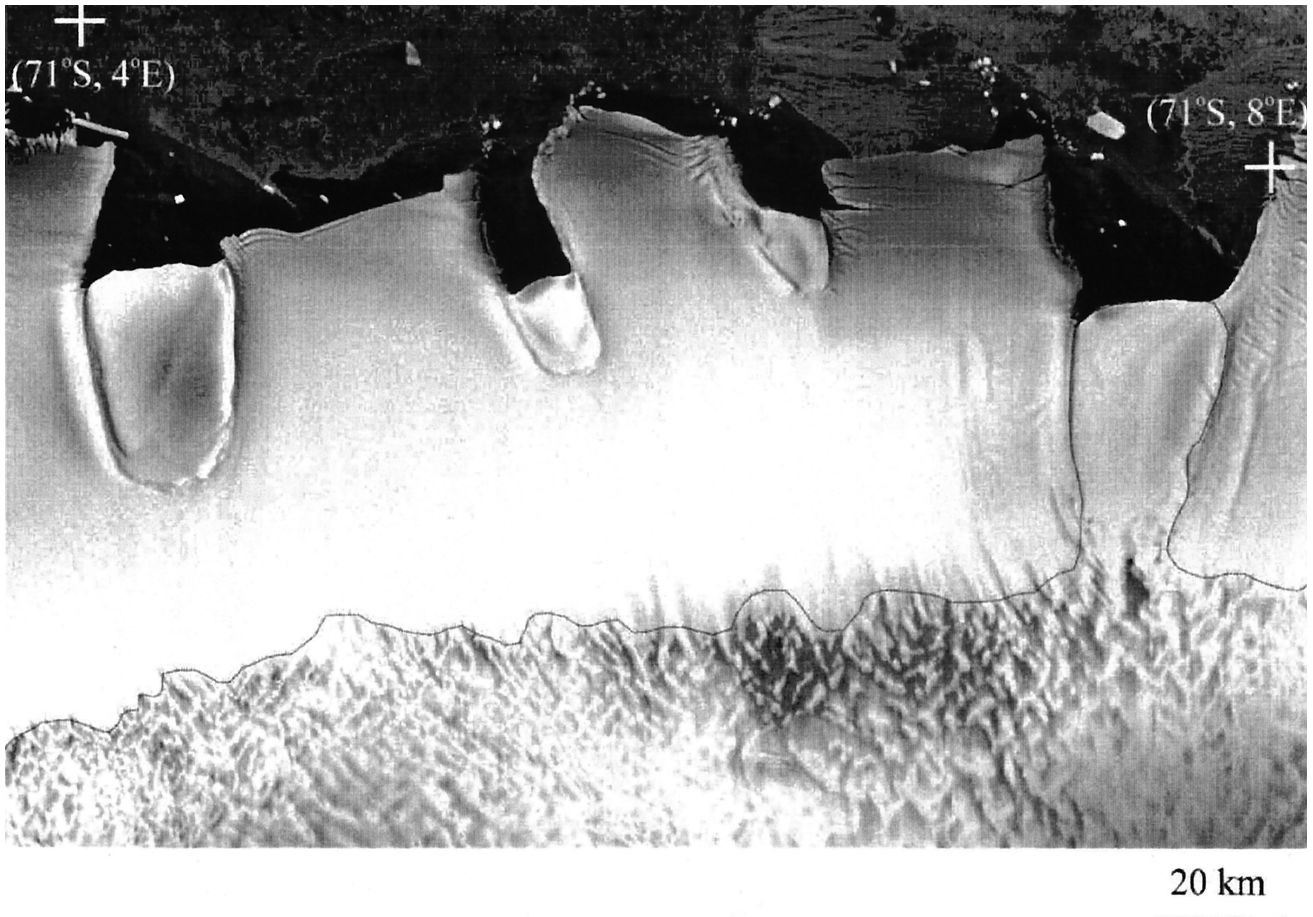


Figure 2. Fimbul Ice Shelf showing the abrupt change in surface texture that we assume delimits the ice shelf grounding line (black line).

1973–1976 Landsat data for the sector from 0° to 36°E longitude. IFAG supplied 1:400,000 scale maps and, on the basis of map accuracy standards [Light, 1993] we take them to have a spatial accuracy of ~120 m. According to *British Antarctic Survey et al.* [1993], the Landsat multispectral scanner data consisted of unrectified photographic products at 1:500,000 scale and registered using tie points to bridge between a limited number of ground control points. This suggests that the relative spatial accuracies of points selected from these data are of the order of several hundred meters. Further, our comparison of ADD and SAR mosaic coastlines suggests that ADD coastlines may be systematically displaced by several kilometers or more depending on the local distribution of geodetic control points used to register the Landsat data. The Landsat data were acquired during the austral summer months.

3.3. Declassified Intelligence Satellite Program

Argon satellite photoreconnaissance data were acquired over our study area between October 29 and November 3, 1963. The high-resolution photographs are preserved on black and white positive film transparencies (4.5 × 4.5 inches). Film resolution is 30 line-pair/mm, and the corresponding spatial resolution (i.e., pixel equivalent) is ~140 m. Individual images cover ~540 × ~540 km. We orthorectified, mosaicked, and enhanced five images as described below.

We scanned the DISP photographs at 7- μ m pixel resolution using the Intergraph PhotoScan TD® Scanner, a high-

resolution radiometrically and geometrically precise flatbed scanning system. A sophisticated photogrammetric and mapping technique using the OSU Antarctic DEM was implemented to derive accurate positional information from the digitized images. This technique used the following collinearity equations as a mathematical model relating image and ground coordinates determined from control points as described later in this section.

$$\begin{aligned} x_{\text{img}} &= x_p \\ &- f \frac{r_{11}(X_{\text{ground}} - X_0) + r_{12}(Y_{\text{ground}} - Y_0) + r_{13}(Z_{\text{ground}} - Z_0)}{r_{31}(X_{\text{ground}} - X_0) + r_{32}(Y_{\text{ground}} - Y_0) + r_{33}(Z_{\text{ground}} - Z_0)} \\ y_{\text{img}} &= y_p \\ &- f \frac{r_{21}(X_{\text{ground}} - X_0) + r_{22}(Y_{\text{ground}} - Y_0) + r_{23}(Z_{\text{ground}} - Z_0)}{r_{31}(X_{\text{ground}} - X_0) + r_{32}(Y_{\text{ground}} - Y_0) + r_{33}(Z_{\text{ground}} - Z_0)}, \end{aligned} \quad (1)$$

where

$x_{\text{img}}, y_{\text{img}}$	measured image coordinates;
x_p, y_p	principal points (assumed to be nadir);
f	focal length (3 inches);
$X_{\text{ground}}, Y_{\text{ground}}, Z_{\text{ground}}$	ground control points;
X_0, Y_0, Z_0	camera positions;
$r_{11}, r_{12}, \dots, r_{33}$	rotation matrix elements as functions of the camera attitude.

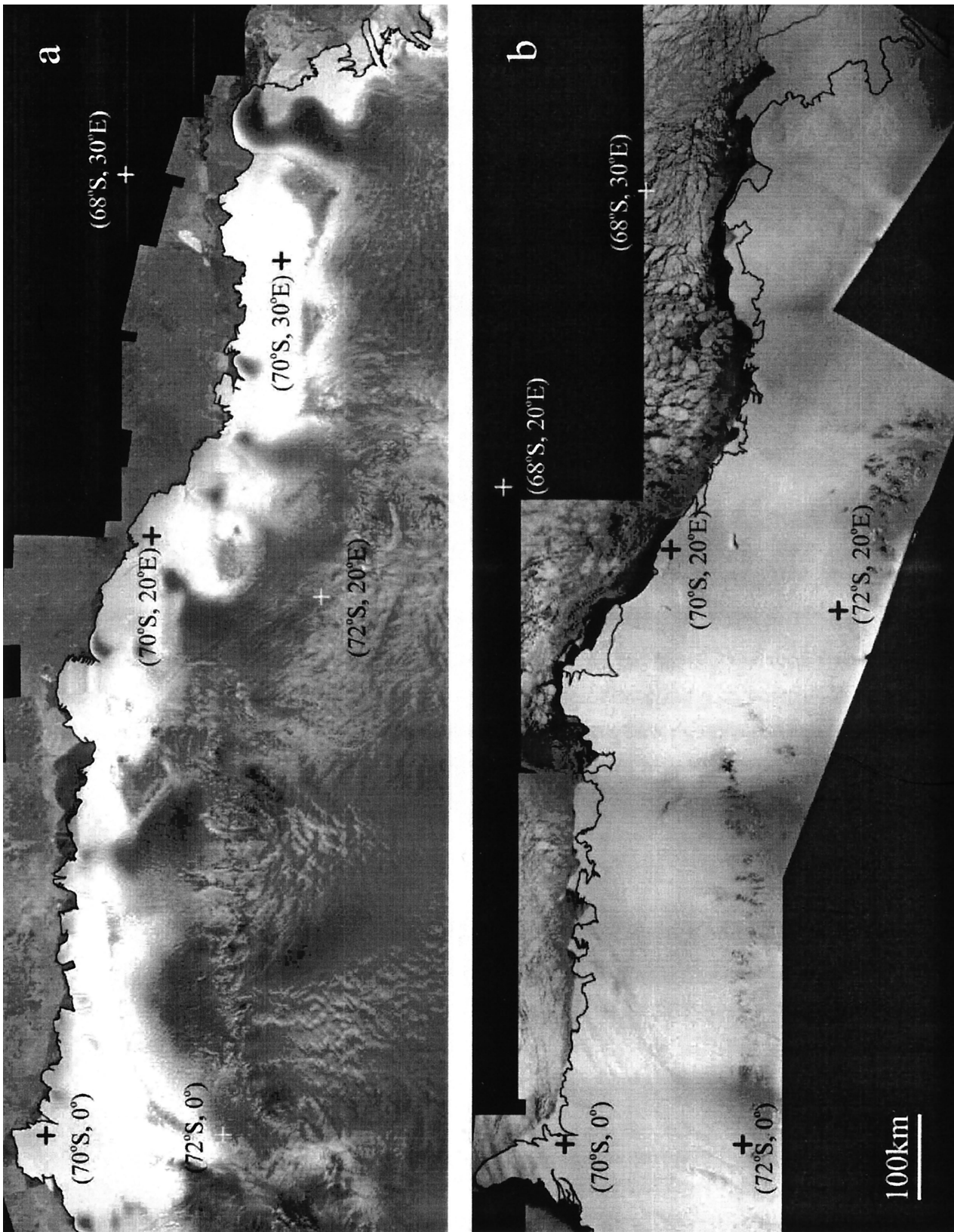


Figure 3. (a) RADARSAT-1 SAR mosaic and inferred ice margin (black line). (b) DISP mosaic and inferred ice margin (black line).

In (1) the measured image coordinates of known control points (CPs) are the observations, and the camera position and attitude (exterior orientation parameters) are unknown parameters. Principal points were estimated from fiducial marks imprinted on the film, which define the image coordinate system. CPs were selected by identifying common features in the georeferenced RADARSAT-1 image mosaic. Horizontal coordinates were estimated from the SAR mosaic, and the corresponding vertical coordinates were taken from the OSU Antarctic DEM. We transformed the CP coordinates from the SAR mosaic, polar stereographic projection into a local three-dimensional (3-D) Cartesian system with a plane tangential to the (WGS84) ellipsoid (available from the World Geodetic Survey 1984 at <http://www.wgs84.com>) at the nadir point. The best fit to (1) was obtained by using a method of least squares that estimates the unknown parameters on the basis of the CPs. The derived exterior orientation parameters (EOPs) served as a basis for orthorectification of the whole image. Finally, the corresponding image coordinates were computed for each DEM cell using (1) with the EOPs and CPs. The irregularly spaced gray values on the resulting polar stereographic projection were converted to a regular image grid through a bilinear interpolation of the irregularly spaced gray values.

We further enhanced the images by removing film grain noise, which contaminates very small-scale, low-contrast images photographed with cameras such as those carried by DISP satellites. The noise is produced by the photographic emulsion during the process of recording an image on film. A common feature of film grain noise is that the power of the noise is related to the brightness of the corrupted pixel. A 2-D adaptive noise removal filter [Lim, 1990, pp. 536–540] was applied to the DISP images. It uses a pixel-wise adaptive Wiener method based on statistics estimated from a local neighborhood of each pixel. A northwest emboss filter, directionally optimized by trial and error, was also applied to portions of several of the images to highlight details further. Figure 4 shows the improvement in image interpretability after noise removal and image enhancement.

The final orthorectified and radiometrically adjusted DISP mosaic is shown in Figure 3b. Exposed mountains are seen poking through the ice sheet in the lower part of the image. Fast ice, dark coastal polynyas, sea ice, and long coastal leads run along the ice shelf margin. First year sea ice floes are distributed across the top of the image.

3.4. DISP Error Assessment

Errors were assessed in two ways. First, least squares analysis using (1) showed that CP geolocation uncertainties of 100 m combined with a 100-m (one pixel) error in locating the CP on the DISP image results in an absolute image geolocation error of 140 m [Kim, 1999]. Second, 15 well-defined common points were measured on the final orthorectified DISP and RADARSAT mosaics to check independently the geolocation of the orthorectified DISP mosaic. The relative rms difference between the two sets of coordinates was <120 m. Combining the relative rms error with the absolute CP error of 100 m gives a second estimate of absolute DISP error of 160 m. We take this more conservative figure as the absolute geolocation error.

4. Analysis and Results

Ice shelf margins were manually derived from the RADARSAT-1 and DISP mosaics. Ice margin mapping was relatively

simple using the SAR data because the glacier ice appears substantially brighter than either seasonal or fast ice. The DISP data were more difficult to interpret because there was very little contrast between glacier ice and fast ice and there was substantially more fast ice cover in 1963 than in 1997. Consequently, we inspected detailed enlargements of the fast ice-dominated DISP data and took subtle curvilinear shadows to be the ice shelf margin (Figure 4). We also relied on characteristic features (such as crevasses, rifts, and icebergs) to distinguish continuous ice shelf from fast ice. The region around Shirase Glacier was the most difficult to interpret because of the combination of ice shelf, ice tongues, icebergs, and fast ice; consequently, we have less confidence in our results for this sector. We estimated position errors using $\sqrt{\sigma_{\text{image}}^2 + \sigma_{\text{picking}}^2}$, where σ_{image} is the horizontal accuracy of the orthorectified image map and σ_{picking} is the error in identifying ice margin positions on the orthorectified image map. We estimate the horizontal accuracies of the DISP and SAR image maps to be ~ 160 and ~ 100 m, respectively. We estimate the picking accuracies of the DISP and SAR ice margins to be 200 and 100 m, respectively, noting that the DISP picking accuracy may be >300 m where fast ice adjoins glacier ice. We estimate absolute ice margin accuracies to be ~ 140 m for the SAR and ~ 260 m for the DISP data. Because there is good contrast between glacial ice and sea ice (other than fast ice) on both the SAR and DISP images, we conclude that ice margin differences >300 m are significant.

We estimated grounding line positions by identifying long boundaries between smooth and textured patterns in the DISP and SAR image data [Jezek *et al.*, 1999]. We attribute the patterns to local changes in surface slope at the grounding line and to the difference between ice sheet flow over bedrock and ice shelf flow over the ocean. We estimate the picking accuracies of the DISP and SAR grounding lines to be 500 and 300 m, respectively. The resulting DISP and SAR grounding line accuracies are 525 and 320 m, respectively. These error estimates do not take into account differences arising from the fact that the microwave image and optical image signature of the grounding line may be different. For that reason we assume that grounding line position differences <1 km are not significant.

Figure 5 shows ice margin and grounding line positions in 1963 and 1997. Also included are ice margin and grounding line positions from the ADD. Regions of ice margin retreat are shaded and regions of advance are shown in black. The most extensive retreat corresponds to the 1967 calving of Trolltunga iceberg that may have been precipitated by the collision of iceberg 1967B with the ice tongue [Swithinbank *et al.*, 1977]. Some of the remaining areas of ice shelf retreat, especially between 0° and 15°E longitude, are associated with the areas between ice rises (hatched areas in Figure 5). The only substantial areas of ice margin advance occur near 20°E longitude in the outflow of Borchgrevinkisen. We find that grounding line positions are not significantly different among our observations for the sector between 0° and 16°E longitude. (We attribute the differences between the 1963/1997 and the 1970s ADD grounding lines across Jutulstraumen Glacier to differences in the interpretation of the image data sets.) For the eastern sector of our study area in the vicinity of Byrdbrean (Figure 1) we find that grounding lines advanced 2.3 km, which seems to be a statistically significant advance. However, we caution again that there could be unaccounted for systematic biases in our grounding line estimates because of differences

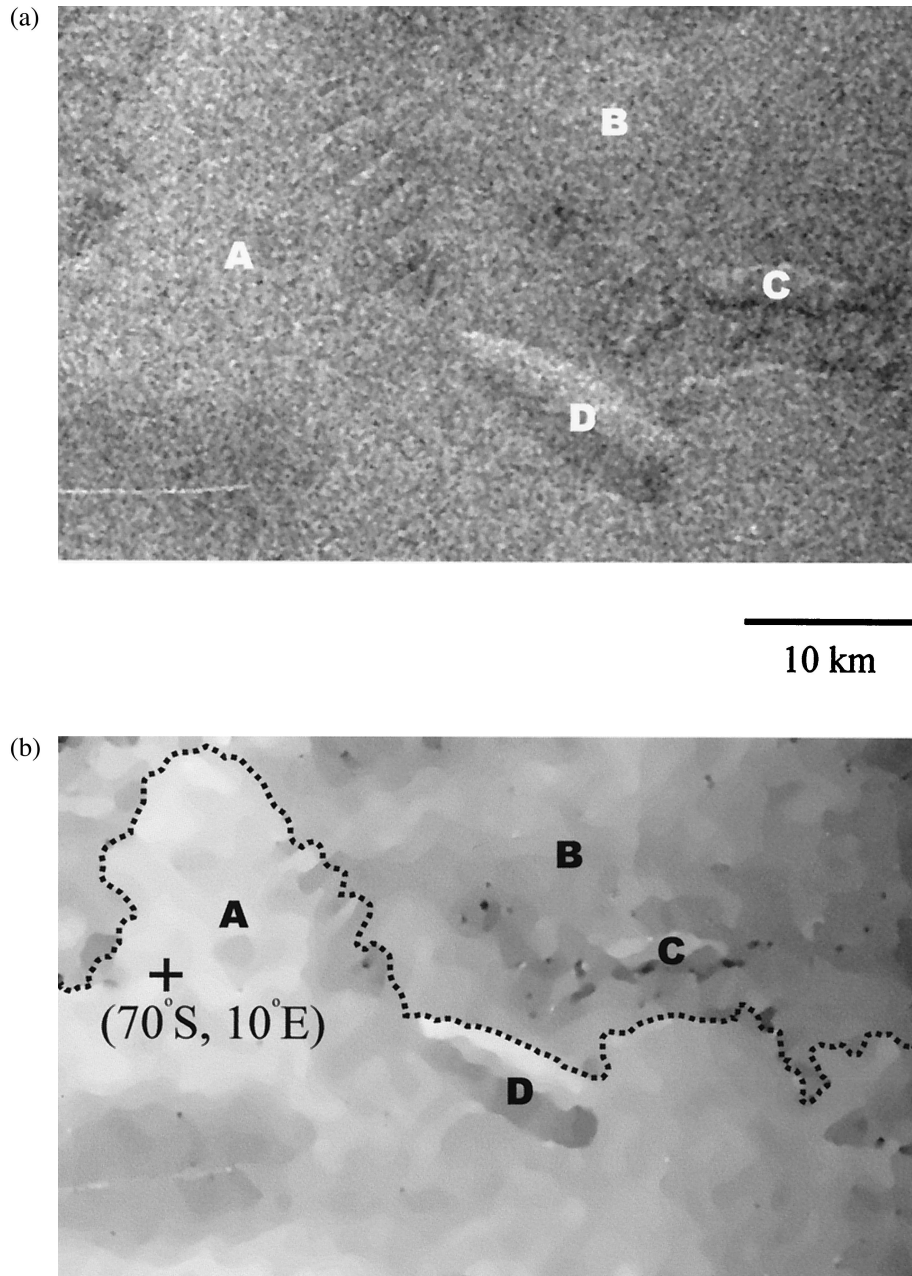


Figure 4. (a) DISP image data after noise removal. (b) DISP image data after application of a northwest emboss filter. The dotted line in Figure 4b corresponds to our estimate of the ice margin. A is glacier ice; B is fast ice; C is iceberg; and D is ice rise.

between the microwave and optical representation of the grounding line.

Combined areal extents of the 1963 ice shelves and ice rises were produced on the basis of the DISP-inferred ice margin and grounding line positions. Combined areal extents of the 1997 ice shelves and ice rises were produced on the basis of the RADARSAT-inferred ice margin and grounding line positions. Table 1 shows ice shelf area and changes in ice shelf area subdivided by drainage systems identified by *Liu et al.* [1999, Figure 4] and includes estimates using ADD data. Calculating the ice shelf area (including ice rises that account for 6604 km² as measured on the RADARSAT-1 data within our study area), we find that the Queen Maud Land ice shelves covered

126,700 km² in 1963 and 118,000 km² in 1997. Net ice shelf loss is thus ~8700 km² or ~6.8% of the total area. This is about twice the area lost by the northern Larsen Ice Shelf in 1995 [Rott *et al.*, 1996]. As an aside, we find that the net area of ice shelf advance (the sum of the black areas in Figure 5) is ~3300 km².

Figure 6 shows our calculated changes in ice margin position along with the latitude of the northerly extent of the ice shelves in 1963. Between 0° and 15°E longitude, ice shelves retreated on average 5.8 km (or >9 km if the Jutulstraumen outflow is included). The more northerly portions of ice shelves and ice tongues retreated the most. The portion of ice margin east of 16°E longitude was on average unchanged.

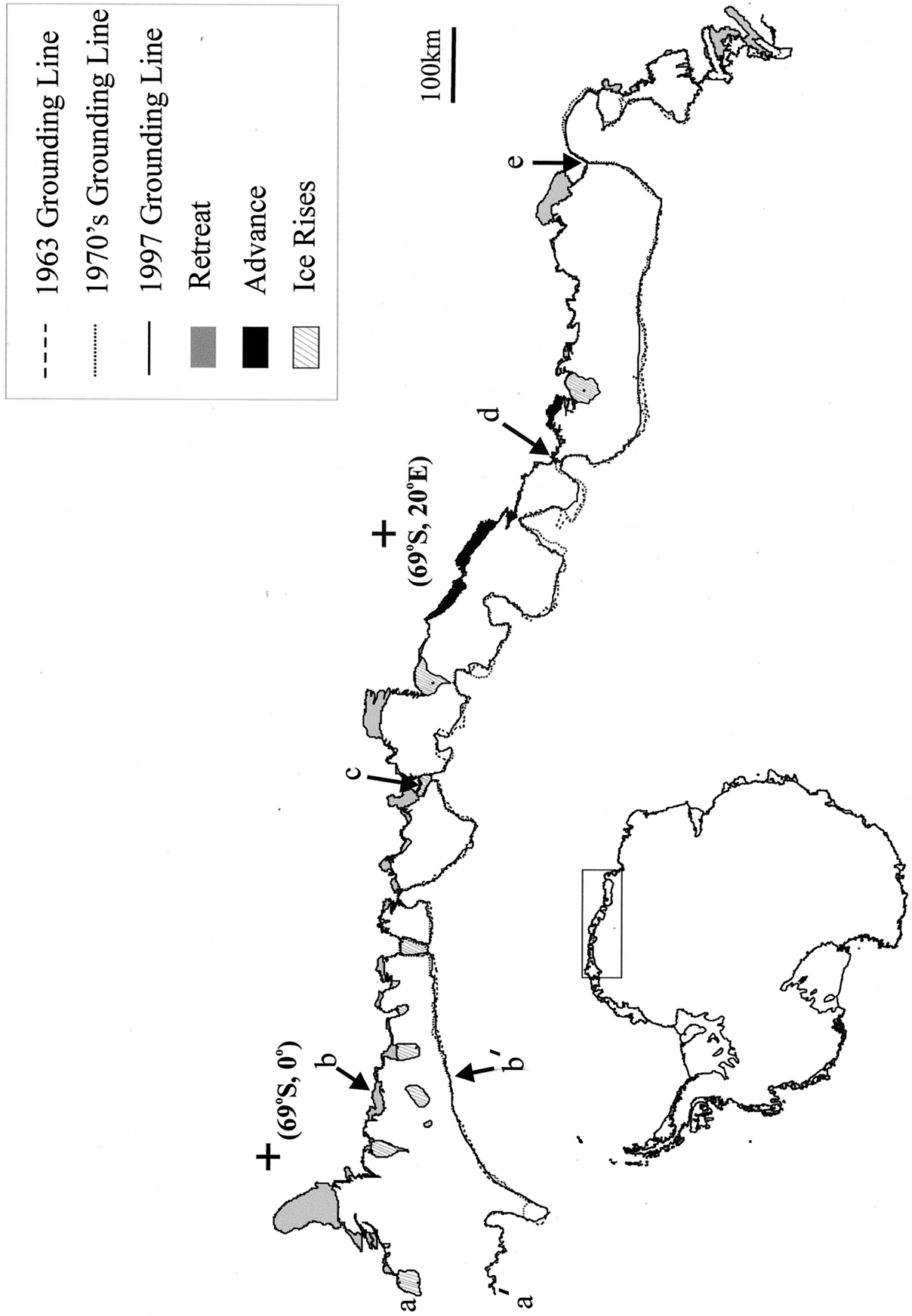


Figure 5. Map illustrating regions of ice shelf retreat (shaded), ice shelf advance (black), and ice rises (hatched) based on comparison of 1963 DISP and 1997 RADARSAT-1 imagery. Lowercase letters delimit the approximate frontal boundaries of drainage basins discussed in Table 1. Grounding line positions for all three data sets discussed in this paper are also shown.

Table 1. Areas and Changes in the Areas of Ice Shelves Partitioned by Local Drainage Systems^a

Year	Drainage Basin Systems				Net
	a-b	b-c	c-d	d-e	
	<i>Areas</i>				
1963	39,187	21,452	30,614	35,420	126,673
1974	34,242	20,021	30,433	34,031	118,727
1997	35,125	19,360	30,491	33,056	118,032
	<i>Changes in Areas (% Change)</i>				
1963–1974	4,945 (12.6)	1,431 (6.7)	181 (0.5)	1,389 (3.9)	7,946 (6.2)
1963–1997	4,062 (10.5)	2,092 (9.7)	123 (0.4)	2,364 (6.7)	8,641 (6.8)

^aMeasurements are in km². Areas in each column correspond to local drainage basins as marked by the lowercase letters (a–e) in Figure 5, identified by Liu *et al.* [1999, Figure 4].

To address partly the question of whether our observed patterns of advance and retreat are episodic or systematic, we plot the 1963, 1997, and ADD ice margins on an enlarged scale in Figure 7. Two facts are revealed by this comparison. First, ice shelves retreated mostly between 1963 and mid-1975. Jutulstraumen Glacier in the west, Lazarev Ice Shelf in the center, and the ice shelf adjacent to Vestvika Bay (32°E longitude) in the east of our study area all retreated between 1963 and the 1970s. Second, ice shelf margin locations from the mid-1970s

to 1997 are very similar (we take the difference between the mid-1970s and the 1997 position of the Riiser-Larsen Peninsula ice wall as a measure of the uncertainty in the ADD geolocation). Jutulstraumen Glacier readvanced slightly between mid-1975 and 1997, as did the Lazarev Ice Shelf. Vestvika Bay ice shelves showed no trend from 1975 to 1997. In contrast, the ice margin advanced between 18° and 26°E longitude and showed a consistent trend between our three observations of 1963, 1975, and 1997.

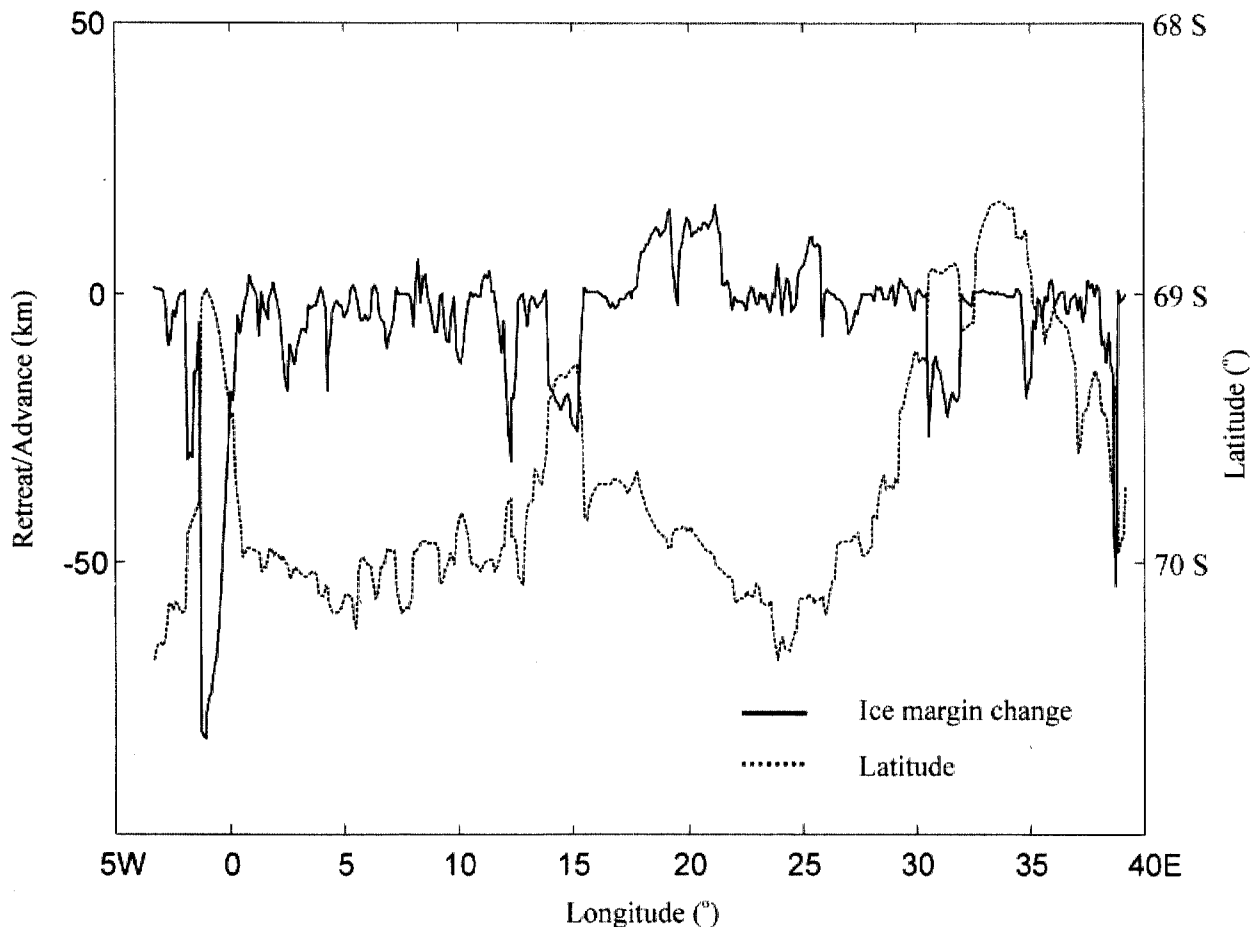


Figure 6. Graph illustrating the magnitude of ice shelf advance/retreat for the period 1963–1997 in relation to the ice shelf northerly extent as measured in 1963.

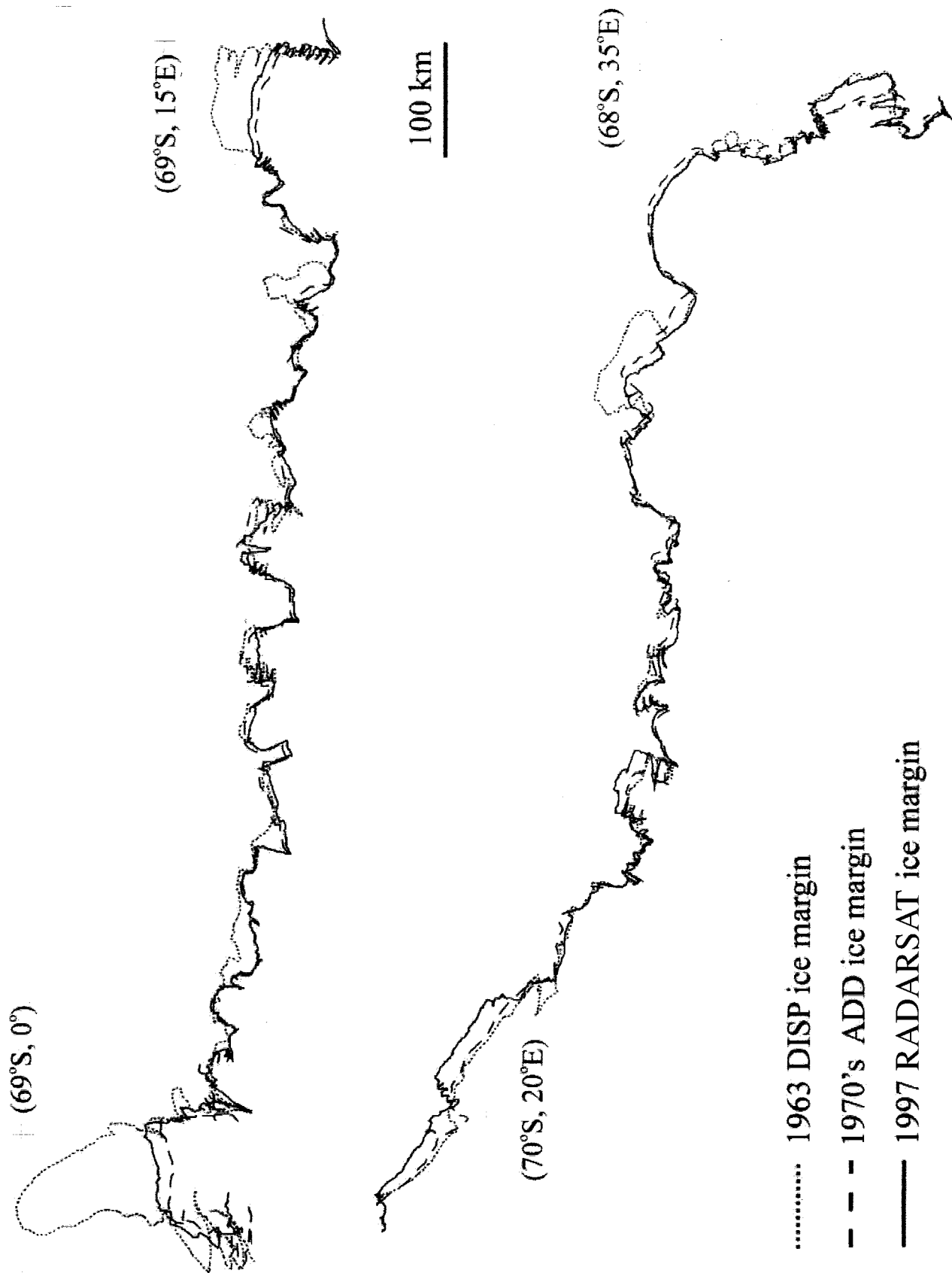


Figure 7. Comparison of coastline estimates from 1963 DISP data (dotted line), mid-1970s Landsat data (dashed line), and 1997 RADARSAT data (solid line).

5. Conclusion

We have shown that Queen Maud Land ice shelves retreated during the 34-year period from 1963 to 1997. We find that most of this retreat occurred between 1963 and 1975. The large unconstrained ice shelves and ice tongues experienced the most retreat. We found little evidence for consistent trends between 1975 and 1997. This observation seems to be consistent with Mercer's [1978] original hypothesis. While these ice shelves are configured similarly to the Antarctic Peninsula ice shelves and, in fact, are experiencing a slight warming trend, the colder summer and mean annual temperatures will tend to stabilize ice margin positions. On the basis of the measured mean annual temperatures at coastal stations, extrapolated measured temperature trends, and the taking of a mean annual temperature of -5°C as a stability criterion [Doake and Vaughan, 1991] we predict that these ice shelves will remain stable for several hundred years.

Acknowledgments. This work was supported by a grant from NASA's Polar Oceans and Ice Sheets Program. RADARSAT-1 imagery is copyrighted by the Canadian Space Agency. BPRC contribution 1201.

References

- British Antarctic Survey, Scott Polar Research Institute, and WCMC, *Antarctic Digital Database User's Guide and Reference Manual*, edited by J. W. Thomson, 56 pp., Sci. Comm. on Antarct. Res., Cambridge, England, U.K., 1993.
- Cooper, A. P. R., J. W. Thomson, and E. M. Edwards, An Antarctic GIS: The first step, *GIS Eur.*, 2, 26–28, 1993.
- Doake, C. S. M., and D. G. Vaughan, Rapid disintegration of the Wordie Ice Shelf in response to atmospheric warming, *Nature*, 350, 328–330, 1991.
- Fahnestock, M., R. A. Bindschadler, R. Kwok, and K. C. Jezek, Greenland ice sheet surface properties and ice dynamics from ERS-1 SAR imagery, *Science*, 262, 1530–1534, 1993.
- Ferrigno, J. G., R. S. Williams Jr., C. E. Rosanova, B. K. Lucchitta, and C. Swithinbank, Analysis of coastal change in Marie Byrd Land and Ellsworth Land, West Antarctica, using Landsat imagery, *Ann. Glaciol.*, 27, 33–40, 1998.
- Jacka, T. H., and W. F. Budd, Detection of temperature and sea-ice-extent changes in the Antarctic and Southern Ocean, 1949–96, *Ann. Glaciol.*, 27, 553–559, 1998.
- Jacobs, S. S., and J. C. Comiso, A recent sea-ice retreat west of the Antarctic Peninsula, *Geophys. Res. Lett.*, 20(12), 1171–1174, 1993.
- Jezek, K. C. (Ed.), RADARSAT Antarctic Mapping Project, in *Proceedings of the Post Antarctic Imaging Campaign-1 Working Group Meeting, BPRC Rep. 17*, 40 pp., Byrd Polar Res. Cent., The Ohio State Univ., Columbus, 1998.
- Jezek, K. C., Glaciological properties of the Antarctic Ice Sheet from RADARSAT-1 synthetic aperture radar imagery, *Ann. Glaciol.*, 29, 286–290, 1999.
- Jezek, K. C., H. Liu, Z. Zhao, and B. Li, Improving a digital elevation model of Antarctica using radar remote sensing data and GIS techniques, *Polar Geogr.*, 23(3), 185–200, 1999.
- Kim, K., Application of time series satellite data to earth science problems, M.S. thesis, 69 pp., The Ohio State Univ., Columbus, 1999.
- King, J. C., and J. Turner, *Antarctic Meteorology and Climatology*, 409 pp., Cambridge Univ. Press, New York, 1997.
- Light, D. L., The National Aerial-Photography Program as a geographic information system resource, *Photogramm. Eng. Remote Sens.*, 59(1), 61–65, 1993.
- Lim, J. S., *Two-Dimensional Signal and Image Processing*, 694 pp., Prentice-Hall, Old Tappan, N. J., 1990.
- Liston, G. E., J. Winther, O. Bruland, H. Elvehøy, K. Sand, and L. Karlöf, Snow and blue-ice distribution patterns on the coastal Antarctic Ice Sheet, *Antarct. Sci.*, 12(1), 69–79, 2000.
- Liu, H., K. C. Jezek, and B. Li, Development of an Antarctic digital elevation model by integrating cartographic and remotely sensed data: A geographic information system-based approach, *J. Geophys. Res.*, 104(B10), 23,199–23,213, 1999.
- McDonald, R. A., Corona: Success for space reconnaissance, a look into the cold war, and a revolution for intelligence, *Photogramm. Eng. Remote Sens.*, 61, 689–720, 1995.
- Mercer, J. H., West Antarctic Ice Sheet and CO₂ greenhouse effect: A threat of disaster, *Nature*, 271, 321–325, 1978.
- Noltimier, K. F., K. C. Jezek, H. G. Sohn, B. Li, H. Liu, F. Baumgartner, V. Kaupp, J. C. Curlander, B. Wilson, and R. Onstott, RADARSAT Antarctic mapping project—mosaic construction, in *IGARSS '99 Proceedings: Remote Sensing of the System Earth—A Challenge for the 21st Century*, pp. 2349–2351, Inst. of Electr. and Electron. Eng., New York, 1999.
- Orheim, O., Glaciological studies by Landsat imagery of perimeter of Dronning Maud Land, Antarctica, *Norsk Polarinst. Skr.*, 169, 69–80, 1978.
- Rott, H., P. Skvarca, and T. Nagler, Rapid collapse of northern Larsen Ice Shelf, Antarctica, *Science*, 271, 788–792, 1996.
- Skvarca, P., W. Rack, and H. Rott, 34 year satellite time series to monitor characteristics, extent and dynamics of Larsen B Ice Shelf, Antarctic Peninsula, *Ann. Glaciol.*, 29, 255–260, 1999.
- Swithinbank, C. W. M., Antarctica, *U.S. Geol. Surv. Prof. Pap.*, 1386-B, 83–96, 1988.
- Swithinbank, C. W. M., P. E. McClain, and P. Little, Drift tracks of Antarctic icebergs, *Polar Rec.*, 18(116), 495–500, 1977.
- Thomson, J. W., and A. P. R. Cooper, The SCAR Antarctic digital topographic database, *Antarct. Sci.*, 5(3), 239–244, 1993.
- Tolstikov, Y. I. (Ed.), *Atlas Antarktiki*, vol. I, 225 pp., Main Admin. of Geod. and Cartogr. of the Minist. of Geol., USSR, Moscow, Russia, 1966.
- Weller, G., Regional impacts of climate change in the Arctic and Antarctic, *Ann. Glaciol.*, 27, 543–552, 1998.
- Zwally, H. J., S. N. Stephenson, R. A. Bindschadler, and R. H. Thomas, Antarctic ice-shelf boundaries and elevations from satellite radar altimetry, *Ann. Glaciol.*, 9, 229–235, 1987.

K. C. Jezek, K. T. Kim, and H. G. Sohn, Byrd Polar Research Center, 108 Scott Hall, 1090 Carmack Road, Columbus, OH 43210. (jezek@iceberg.mps.ohio-state.edu; kim.933@osu.edu; sohn1@yonsei.ac.kr)

(Received March 21, 2000; revised December 8, 2000; accepted December 22, 2000.)